JOURNAL OF SPACECRAFT AND ROCKETS
Vol. 42, No. 5, September–October 2005

Optimal Invariant Spacecraft Formation Deployment with Collision Risk Management

A. Boutonnet* and V. Martinot†
Alcatel Space, 31037 Toulouse, France
A. Baranov‡
Russian Academy of Sciences, 125047, Moscow, Russia
and
B. Escudier§
Higher National School for Aeronautics and Space, 31055 Toulouse, France

The analytical solution of the deployment phase of a spacecraft formation is provided. The solution applies to Earth-centered invariant formations. These feature a fixed geometry over one revolution, which renders them useful for numerous purposes, especially radar interferometry and sparse aperture synthesis. First, a formulation useful for formation design is defined in terms of nonsingular elements. This is used as a basis for solving the deployment phase. The primer vector theory is applied to obtain the minimal fuel consumption. Next, this theory is combined with a geometrical approach to yield the maneuver components of the optimal solution. In addition, the payload separation strategy from the rocket upper stage is also optimized to take into account the collision risk.

Nomenclature

a	=	semimajor axis, km
e	=	eccentricity
$\boldsymbol{e}$	=	eccentricity vector
i	=	inclination, rad
$\boldsymbol{i}$	=	inclination vector
k_j	=	formation shape constants
M	=	mean anomaly, rad
$\mathcal{R}$	=	inertial equatorial frame
$\mathcal{R}_{\text{loc}}$	=	local orbital frame
$\mathcal{R}'$	=	inertial frame linked to the reference orbit
v	=	true anomaly, rad
$\bar{x}$	=	with respect to the reference orbit
$\tilde{x}$	=	normalized variable
$\hat{\boldsymbol{x}}$	=	unit vector
α	=	mean argument of the latitude, rad
$\boldsymbol{\Delta V}$	=	impulsive maneuver, km/s
η	=	separation impulse ratio
θ	=	formation phase angle, rad
λ'	=	angle along the orbit measured from the reference right ascension of the ascending node (RAAN), rad
ρ	=	formation size parameter, km
Ω	=	RAAN, rad
ω	=	argument of perigee, rad

Introduction

FORMATION flying is an enabling technology for innovative missions. Numerous applications, for example, radar interferometry or antenna synthesis, benefit[1] from a special class of Earth-centered formations: the invariant or free elliptical formations.[2,3] The interesting feature of these formations is that the natural relative motion of a spacecraft around the reference orbit is elliptical. Reconfiguration of such formations, for example; deployment, size, and shape change, has been extensively studied. However, the related optimization problem is usually solved by means of heuristics (number and location of maneuvers, type of components) and gives near-optimal solutions whose optimality must be checked a posteriori.[4–6] We propose here to apply optimal control theory to find the optimal solution for the deployment phase analytically. Our solution takes into account the collision risk by addressing and optimizing the formation spacecraft separation strategy from the rocket upper stage.

The input to the optimization problem is the targeted changes in the orbital elements. These follow from the requirements defined by the target formation. Several models already exist for the invariant formation design. Sabol et al.[7] proposed the first model for circular and projected circular formations in terms of Cartesian elements in an inverse square law field. New models based on Keplerian classical elements considering various orbital perturbation sources have been proposed (see Refs. 8–10). However, the optimal control theory employed in our method requires the model to be given in terms of Keplerian nonsingular elements.

Hence, the next section of this paper concentrates on the formation model design. The obtained model is then used in the third section to formulate the optimization problem. The fourth section introduces the optimal control theory and the geometrical approach to obtain the analytical optimal solution to the deployment phase. Finally, in the last section before the Conclusions section, a numerical example is given.

Formation Design

The reference orbit state vector is defined as

$$\bar{\boldsymbol{\chi}} \equiv [\bar{a}, \bar{e}_x, \bar{e}_y, \bar{i}, \bar{\Omega}, \bar{\alpha}]^T \tag{1}$$

expressed in an inertial frame $\mathcal{R} \equiv \{O, \hat{\boldsymbol{x}}, \hat{\boldsymbol{y}}, \hat{\boldsymbol{z}}\}$, where $\bar{a}$ is the reference semimajor axis, $\bar{\boldsymbol{e}} = [\bar{e}_x = \bar{e}\cos\bar{\omega},\ \bar{e}_y = \bar{e}\sin\bar{\omega}]^T$ the reference eccentricity vector, $\bar{i}$ the reference inclination, $\bar{\Omega}$ the reference right ascension of the ascending node (RAAN), and $\bar{\alpha} = \bar{\omega} + \bar{M}$ the reference mean argument of the latitude. Of particular interest is the state vector of a spacecraft flying close to the reference. It is defined by its deviation $\boldsymbol{\delta\chi}$ with respect to the reference state vector. When the reference orbit is circular and when Keplerian dynamics is assumed,

Presented as Paper 2003-0653 at the AAS/AIAA Astrodynamics Specialists Conference, Big Sky, MT, 3–7 August 2003; received 3 November 2003; revision received 15 November 2004; accepted for publication 24 November 2004.

*Ph.D. Student, 26, Avenue J.F. Champollion; arnaud.boutonne.03@supaero.org. Student Member AIAA.
†Mission Analyst, Mission Analysis Service, Systems and Ground Segment Programs Division, 26, Avenue J.F. Champollion.
‡Leading Scientific Researcher, Scientific Research Department, Keldysh Institute of Applied Mathematics.
§Professor and Head, Space Department, 10, Avenue Edouard Belin.

the motion is invariant[2] if

$$\delta a = 0, \qquad \delta e_x = -(\rho/2\bar{a})\sin\theta$$

$$\delta e_y = (\rho/2\bar{a})\cos\theta, \qquad \delta i = k_1(\rho/\bar{a})\cos\theta$$

$$\delta\Omega = k_1(\rho/\bar{a}\sin\bar{i})\sin\theta, \qquad \delta\alpha = -\cos(\bar{i})\delta\Omega \qquad (2)$$

In this set of equations, ρ is the formation size parameter (equal to the elliptic in-plane projection semimajor axis), θ is a phasing angle, and k_1 is the constant parameter corresponding to the relative motion shape. Figure 1 gives the geometrical representation of these equations in the reference local orbital frame (LOF) $\mathcal{R}_{\text{LOF}} \equiv \{\hat{\boldsymbol{r}}, \hat{\boldsymbol{t}}, \hat{\boldsymbol{n}}\}$, where $\hat{\boldsymbol{r}}$ is the radial direction, $\hat{\boldsymbol{t}}$ is the transversal direction, and $\hat{\boldsymbol{n}}$ is the normal direction. There are two special cases: If $k_1 = \sqrt{3}/2$, the relative motion is circular in $\mathcal{R}_{\text{LOF}}$, and the projected motion onto the plane $(\hat{\boldsymbol{t}}, \hat{\boldsymbol{n}})$ is circular if $k_1 = 1$. Figure 2 shows an example of the orbits of the reference and of the spacecraft to yield a circular motion.

However, this model does not account for reference orbits with small eccentricity ($\bar{e} \approx 10^{-3}$, which is the case for many low-Earth-orbit missions). A series expansion of the true anomaly and of the orbit radius in terms of the mean anomaly[11] shows that this result stands up to first order in eccentricity. This is derived in Ref. 12.

Moreover, this model is not valid for reference orbits with small inclination, which is the case for geosynchronous-Earth-orbit formations because $\delta\Omega$ tends to be infinite. To solve this difficulty, the inclination vector $\bar{\boldsymbol{i}}$ is introduced. It is defined as $\bar{\boldsymbol{i}} \equiv [\bar{i}_x = \sin\bar{i}\cos\bar{\Omega}\,,\ \bar{i}_y = \sin\bar{i}\sin\bar{\Omega}]^T$. Then it is possible to derive[12] the new set of equations describing the formation geometry:

$$\delta a = 0, \qquad \delta e_x = -(\rho/2\bar{a})\sin\theta$$

$$\delta e_y = (\rho/2\bar{a})\cos\theta, \qquad \delta i_{x_1} = k_1(\rho/\bar{a})\cos\bar{i}\cos\theta$$

$$\delta i_{y_1} = k_1(\rho/\bar{a})\sin\theta, \qquad \delta\alpha = -\cos(\bar{i})\delta\Omega \qquad (3)$$

Of particular interest is the geometrical representation of the targeted changes in the spacecraft orbital elements with respect to the reference orbit as shown in Fig. 3a. Figure 3a clearly shows that the

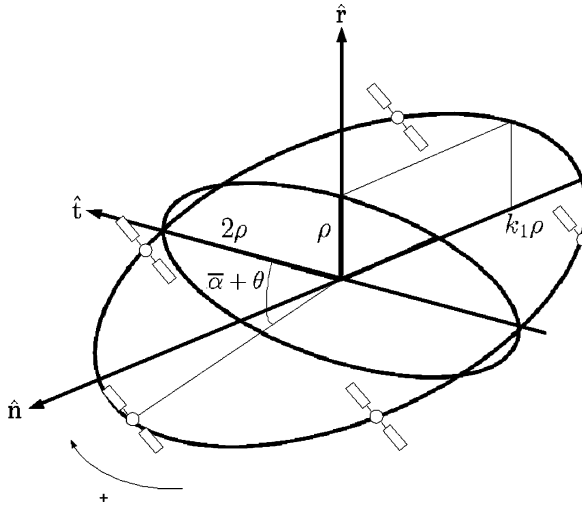

Fig. 1 Invariant formation design in local orbital frame of reference orbit.

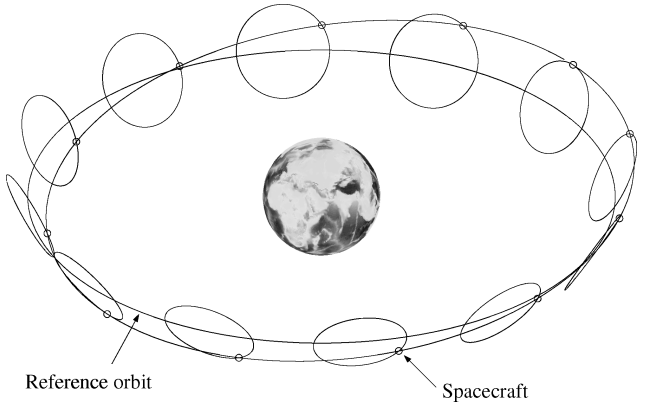

Fig. 2 Example of orbit corresponding to a relative circular motion.

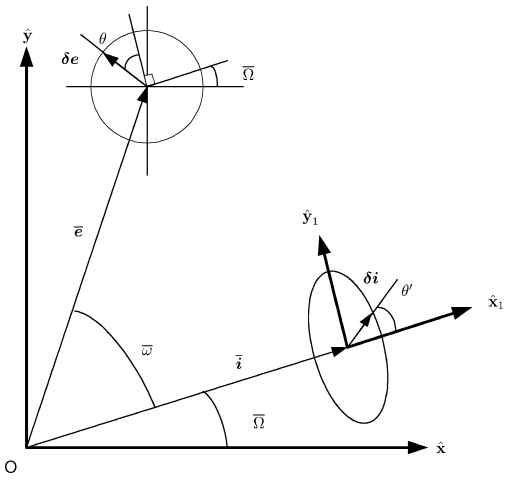

a) Reference orbit with intermediate inclination, for example, 50 deg

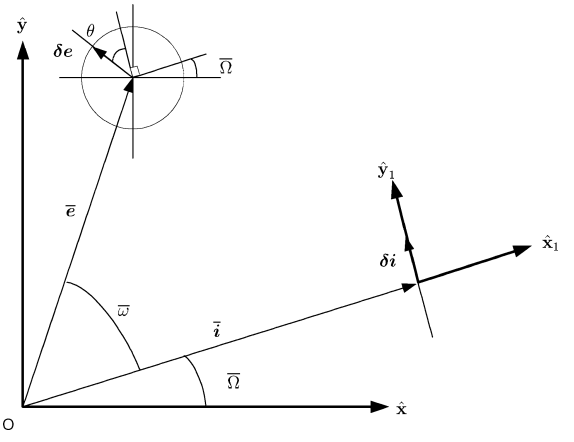

b) Polar reference orbit case

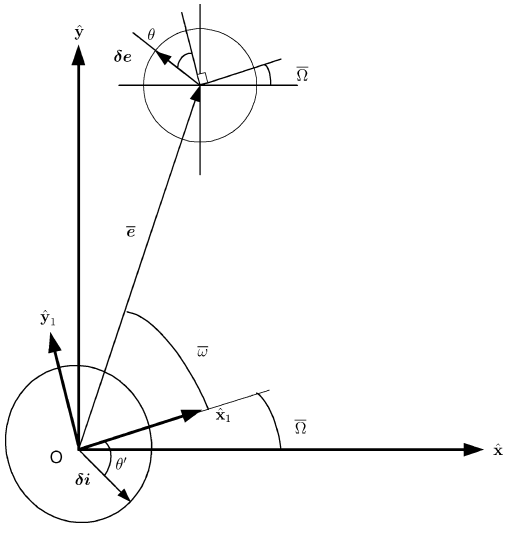

c) Equatorial reference orbit case

Fig. 3 Geometrical representation of invariant formations.

eccentricity vector change is a circle and that the inclination vector change is an ellipse.

A new set of axes have been introduced: $\hat{\boldsymbol{x}}_1, \hat{\boldsymbol{y}}_1$, and $\hat{\boldsymbol{z}}_1$ are derived from $\hat{\boldsymbol{x}}, \hat{\boldsymbol{y}}$, and $\hat{\boldsymbol{z}}$ by a rotation around $\hat{\boldsymbol{z}}$ equal to $\bar{\Omega}$. The components δi_{x_1} and δi_{y_1} are given with respect to this frame to exhibit the elliptical shape of the inclination vector change in function of θ. When expressed in the same frame as $\bar{\boldsymbol{i}}$, the targeted change is simply

$$\delta i_x = \cos\bar{\Omega}\delta i_{x_1} - \sin\bar{\Omega}\delta i_{y_1}$$

$$\delta i_y = \sin\bar{\Omega}\delta i_{x_1} + \cos\bar{\Omega}\delta i_{y_1} \tag{4}$$

With this representation, $\delta\Omega$ is never infinite, whatever the reference inclination. This is a nonsingular representation.

For nonpolar reference orbits, the angle θ' has a value

$$\theta' = \arctan(\tan\theta/\cos\bar{i}) \tag{5}$$

Two particular cases can be shown from Eq. (3): The first one corresponds to a polar reference orbit, and the second one corresponds to an equatorial reference orbit. The first case is shown in Fig. 3b: The component δi_{x_1} is null. Therefore, the angle θ' is non definite, and the inclination vector change is a segment of a straight line. The second case is shown in Fig. 3c: The targeted inclination vector change is a circle. The model given in Eq. (3) will serve as an input in the following section.

Formulation of the Deployment Problem

The deployment of an invariant formation poses the following problem: All spacecraft are stacked on the upper stage of the rocket. For each spacecraft, the deployment consists in obtaining the changes in the orbital elements given in Eq. (3). Basically, this is a rendezvous between two close near-circular orbits. It is more convenient to solve this task in an inertial frame linked with the reference orbit. The optimization technique that will be used is indeed usually given in such a frame. Therefore, a new set of axes have been introduced: $\hat{\boldsymbol{x}}', \hat{\boldsymbol{y}}'$, and $\hat{\boldsymbol{z}}'$ are derived from $\hat{\boldsymbol{x}}_1, \hat{\boldsymbol{y}}_1$, and $\hat{\boldsymbol{z}}_1$ by a rotation around $\hat{\boldsymbol{x}}_1$ equal to $\bar{i}$.

Given an l-impulse solution, the deployment optimization problem[13] $\mathcal{P}_1$ is

$$(\mathcal{P}_1)\begin{cases} \min \sum_{j=1}^{l} \|\Delta \boldsymbol{V}_j\| \\ \delta\tilde{a} = 0 \\ \delta e_x = -(\rho/2\bar{a})\sin\theta \\ \delta e_y = (\rho/2\bar{a})\cos\theta \\ \delta i'_x = k_1(\rho/\bar{a})\cos\theta \\ \delta i'_y = k_1(\rho/\bar{a})\sin\theta \\ \delta\lambda' = k_2 \end{cases} \tag{6}$$

where λ' is the angle along the orbit between the reference orbit ascending node and the spacecraft.

From problem $\mathcal{P}_1$, it can be deduced that

$$\delta e = \|\delta\boldsymbol{e}\| = \rho/2\bar{a} \tag{7}$$

$$\delta i = \|\delta\boldsymbol{i}'\| = k_1\rho/\bar{a} \tag{8}$$

$$(\delta\boldsymbol{i}', \delta\boldsymbol{e}) = \pi/2 \tag{9}$$

This clearly shows that the deployment problem is independent of θ. If all formation spacecraft have the same size parameter ρ, the optimal solution corresponding to $\mathcal{P}_1$ will be the same for any spacecraft.

Suppose that a transfer $\mathcal{P}_2$, that is, without the constraint $\delta\lambda' = k_2$, is solved instead of a rendezvous. The optimal solution will lead to $\delta\lambda'_j(t_f)$ for spacecraft j. However, because the solution is the same for all spacecraft, $\delta\lambda'_j(t_f)$ will be the same for another spacecraft: By simply solving a transfer, all spacecraft will be deployed on the same invariant formation (with, of course, different phase angles θ).

In a previous paper,[14] it has been shown that the minimum-fuel solution to the problem $\mathcal{P}_2$ led to a collision between all spacecraft and the rocket upper stage from which they were separated. To counteract this problem, one solution consists in introducing a distance constraint and solving the optimization problem a priori [nonconvex nonlinear programming (NLP)]. In this paper, we chose a different solution by finding the optimal deployment for any separation impulse and then adjusting this impulse such that the distance constraint requirement is met. Note that this method will not give the true constrained minimum because, contrary to the NLP solution, the distance constraint is not directly taken into account in the optimization process.

The separation impulse $\Delta\boldsymbol{V} = [\Delta V_r \ \Delta V_t \ \Delta V_n]^T$ will affect the orbital elements. The well-known Gauss variational equations (see Ref. 15) are used in normalized form,

$$\delta\tilde{a} = 2\Delta\tilde{V}_t, \qquad \delta e_x = 2\cos\lambda'\Delta\tilde{V}_t + \sin\lambda'\Delta\tilde{V}_r$$

$$\delta e_y = 2\sin\lambda'\Delta\tilde{V}_t - \cos\lambda'\Delta\tilde{V}_r, \qquad \delta i'_x = \cos\lambda'\Delta\tilde{V}_n$$

$$\delta i'_y = \sin\lambda'\Delta\tilde{V}_n, \qquad \delta\lambda' = -3\Delta\tilde{t}\Delta\tilde{V}_t - 2\Delta\tilde{V}_r \tag{10}$$

Here, the normalized form means that all distances are divided by $\bar{a}$ and that all velocities are divided by the circular velocity $V_{\text{circ}} = \sqrt{(\mu/\bar{a})}$. The normalized variables are denoted with a tilde.

Figure 4 gives the geometrical meaning of these equations: The two vectors $\delta\boldsymbol{e}$ and $\delta\boldsymbol{i}'$ of the problem $\mathcal{P}_2$ are represented in the plane $\{\hat{\boldsymbol{x}}', \hat{\boldsymbol{y}}'\}$. The circle $\mathcal{C}$ whose radius is $\delta\tilde{a}$ is also given. Furthermore, a set of three vectors $\{\boldsymbol{\xi}_r, \ \boldsymbol{\xi}_t, \ \boldsymbol{\xi}_n\}$ representative of the maneuver $\Delta\tilde{\boldsymbol{V}}$ is drawn. We define their coordinates as

$$\boldsymbol{\xi}_r \equiv \left[\Delta\tilde{V}_r \sin\lambda', -\Delta\tilde{V}_r \cos\lambda'\right]^T$$

$$\boldsymbol{\xi}_t \equiv \left[2\Delta\tilde{V}_t \cos\lambda', 2\Delta\tilde{V}_t \sin\lambda'\right]^T$$

$$\boldsymbol{\xi}_n \equiv \left[\Delta\tilde{V}_n \cos\lambda', \Delta\tilde{V}_n \sin\lambda'\right]^T \tag{11}$$

From Fig. 4, it is possible to construct a sequence of maneuvers such that these vectors yield exactly $\delta\boldsymbol{e}$, $\delta\boldsymbol{i}'$, and $\delta\tilde{a}$. This corresponds to the following set of equations:

$$\sum_j \frac{\Delta\tilde{V}_{rj}}{|\Delta\tilde{V}_{rj}|}\|\boldsymbol{\xi}_{rj}\| = \delta\tilde{a}, \qquad \sum_j \boldsymbol{\xi}_{tj} + \boldsymbol{\xi}_{tj} = \delta\boldsymbol{e}$$

$$\sum_j \boldsymbol{\xi}_{nj} = \delta\boldsymbol{i}' \tag{12}$$

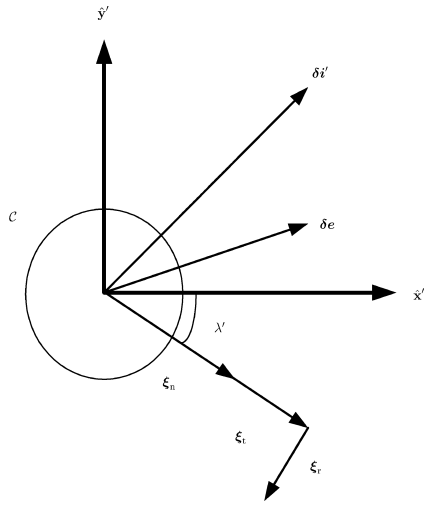

Fig. 4 Geometrical representation of Gauss variational equations.

This geometrical representation allows finding analytical solutions to the deployment problem.

Now, by the choice of a separation strategy, the effect of the separation impulse on the orbital parameters can be derived. A usual strategy[16,17] consists in using a transversal impulse:

$$\boldsymbol{\Delta V}_{\text{sep}} = \Delta V_{\text{sep}} \hat{\boldsymbol{t}} \tag{13}$$

that is freely obtained, for example, with the help of a spring-loaded device.

By combination of Eqs. (6), (10), and (13), the new optimization problem $\mathcal{P}_3$ is

$$(\mathcal{P}_3)\begin{cases} \min \sum_{j=1}^{l} \|\boldsymbol{\Delta}\tilde{\boldsymbol{V}}_j\| \\ \delta\tilde{a} = -2\|\boldsymbol{\Delta}\tilde{\boldsymbol{V}}_{\text{sep}}\| \\ \delta e_x = -(\tilde{\rho}/2)\sin\theta - 2\|\boldsymbol{\Delta}\tilde{\boldsymbol{V}}_{\text{sep}}\|\cos\lambda'_{\text{sep}} \\ \delta e_y = (\tilde{\rho}/2)\cos\theta - 2\|\boldsymbol{\Delta}\tilde{\boldsymbol{V}}_{\text{sep}}\|\sin\lambda'_{\text{sep}} \\ \delta i'_x = k_1\tilde{\rho}\cos\theta \\ \delta i'_y = k_1\tilde{\rho}\sin\theta \end{cases} \tag{14}$$

where λ'_{sep} is the angle where the spacecraft is separated.

Optimization

Primer Vector Approach

The optimization problem $\mathcal{P}_3$ can be solved in various ways, numerically as well as analytically. Numerical solutions are time consuming and sometimes difficult to explain physically. Analytical deployment has been studied by several authors[4–6] and leads to sub- or near-optimal solutions.

What we propose here is a direct use of the optimal impulsive control theory, namely, the primer vector that was introduced by Lawden.[18] Several general results of the primer vector approach will be covered in the following section.

The spacecraft state vector shall be defined by its distance to the attracting body, its velocity, and its mass. When Pontryagin's maximum principle is applied, the costate is adjoined to the dynamics. For an impulsive solution, the necessary conditions of optimality are met when the primer vector (that is, the adjoint of the velocity) trajectory, called the primer locus, is inside or tangential to the unity sphere. Every time it is tangential, an impulse must be applied. The impulse direct cosines are given by the orientation of the primer vector.

Furthermore, when the initial and the final orbits are close, the dynamics can be linearized about a reference orbit. This leads to some simplifications as explained in Refs. 19 and 20. For instance, there are only three kinds of optimal transfers: nodal, nondegenerate, and singular.

The nodal transfer corresponds to a bitangent elliptic primer locus: The optimal solution is two impulsive. The maneuvers are applied along the line of nodes between the initial and the final orbits. The maneuvers' direct cosines are opposite.

The nondegenerate transfer is also two impulsive. The maneuvers' direct cosines are equal for the transversal components (along $\hat{\boldsymbol{t}}$), whereas they are opposite for the radial and normal components.

The singular transfer is more complicated: The primer locus is circular, and, as a consequence, it is always tangential to the unity sphere. Hence, the number and the location of maneuvers is unknown.

By the definition of $\delta e_{//}$ as the projection of $\boldsymbol{\delta e}$ onto $\boldsymbol{\delta i'}$, and with $\delta e_{\perp}$ as its orthogonal projection, a transfer is nodal if and only if

$$\delta i'^2 \geq 3\delta e_{\perp}^2 \tag{15a}$$

$$\delta\tilde{a}^2 \leq \delta e_{//}^2 \tag{15b}$$

The related optimal fuel consumption is

$$\Delta\tilde{V} = \sqrt{\delta i^2 + \delta e_{//}^2/4 + \delta e_{\perp}^2} \tag{16}$$

It is nondegenerate if and only if

$$\delta\tilde{a}^2 \geq \delta e_{//}^2 \tag{17a}$$

$$\delta\tilde{a}^2 \leq \delta e^2 + \left(2/\sqrt{3}\right)\delta e_{\perp}\delta i' - \delta i'^2 \tag{17b}$$

The optimal fuel consumption for this case is

$$\Delta\tilde{V} = \Big(\delta i^2 + \delta e^2 - \tfrac{1}{2}\delta\tilde{a}^2 + \sqrt{(\delta i^2 - \delta e^2 + \delta\tilde{a}^2)^2 + 4\delta i^2\delta e_{\perp}^2}\Big)^{\frac{1}{2}}\Big/\sqrt{2} \tag{18}$$

Finally, it is singular if and only if

$$\delta\tilde{a}^2 \leq \delta e^2 + \left(2/\sqrt{3}\right)\delta e_{\perp}\delta i' - \delta i'^2 \tag{19a}$$

$$\delta i'^2 \leq 3\delta e_{\perp}^2 \tag{19b}$$

For this latter case, the optimal fuel consumption is

$$\Delta\tilde{V} = \sqrt{\delta e_{//}^2 + \left(\delta e_{\perp} + \sqrt{3}\delta i\right)^2}\Big/2 \tag{20}$$

The separation impulse induces a residual eccentricity vector $\boldsymbol{\delta e}_{\text{res}}$ and a semimajor axis change $\delta\tilde{a}$. They are shown in Fig. 5 with $\boldsymbol{\xi}_{\text{sep}} = \boldsymbol{\Delta}\tilde{\boldsymbol{V}}_{\text{sep}}/2$. Together with $\mathcal{P}_3$, Fig. 5 allows calculation of the target corrections:

$$\delta\tilde{a} = -2\|\boldsymbol{\Delta}\tilde{\boldsymbol{V}}_{\text{sep}}\|$$

$$\|\boldsymbol{\delta e}_{\text{res}}\| = \sqrt{\|\boldsymbol{\delta e}\|^2 + 4\|\boldsymbol{\Delta}\tilde{\boldsymbol{V}}_{\text{sep}}\|^2 - 4\|\boldsymbol{\delta e}\|\|\boldsymbol{\Delta}\tilde{\boldsymbol{V}}_{\text{sep}}\|\sin(\lambda'_{\text{sep}} - \theta)}$$

$$\delta e_{\text{res}\perp} = \|\boldsymbol{\delta e}\| - 2\|\boldsymbol{\Delta}\tilde{\boldsymbol{V}}_{\text{sep}}\|\sin(\lambda'_{\text{sep}} - \theta)$$

$$\delta e_{\text{res}//} = -2\|\boldsymbol{\Delta}\tilde{\boldsymbol{V}}_{\text{sep}}\|\cos(\lambda'_{\text{sep}} - \theta)$$

$$\|\boldsymbol{\delta i'}\| = 2k_1\|\boldsymbol{\delta e}\| \tag{21}$$

By combining Eq. (21) with the primer vector bounds, we have shown that the transfer is nondegenerate. Thus, the optimal consumption $\Delta\tilde{V}^*$ is given by Eq. (18).

The optimal consumption is a function of two variables: the separation impulse angle λ'_{sep} and the separation impulse amplitude $\|\boldsymbol{\Delta}\tilde{\boldsymbol{V}}_{\text{sep}}\|$. First, we calculate the optimal value λ'^*_{sep} by deriving

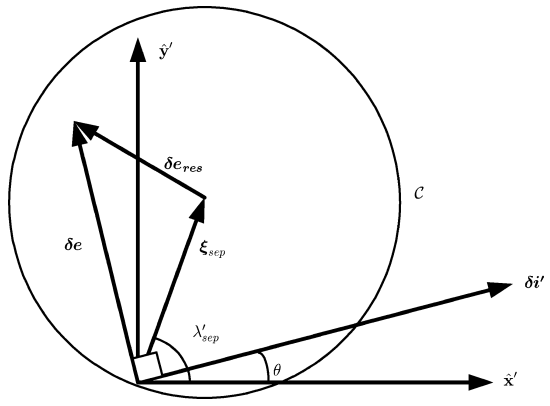

Fig. 5 Deployment problem geometrical representation.

$\partial_{\lambda'_{\text{sep}}}(\Delta\tilde{V}^*)=0$. Two roots are found:

$$\lambda'^*_{\text{sep1}} = 2n_{\text{sep}}\pi + \pi/2 + \theta$$

$$\lambda'^*_{\text{sep2}} = 2n_{\text{sep}}\pi + \arctan(4\eta^2-1)^{-\frac{1}{2}} + \theta \tag{22}$$

where n_{sep} is an integer. The second root depends on the very important ratio η

$$\eta \equiv \|\boldsymbol{\Delta}\tilde{\boldsymbol{V}}_{\text{sep}}\| \,/\, \|\boldsymbol{\delta e}\| \tag{23}$$

The second-order necessary condition of optimality $\partial^2_{\lambda'_{\text{sep}}}(\Delta\tilde{V}^*)>0$ allows derivation of the following intervals:

$$0<\eta<1/2: \quad \lambda'^*_{\text{sep}} = \lambda'^*_{\text{sep1}}$$

$$\eta>1/2: \quad \lambda'^*_{\text{sep}} = \lambda'^*_{\text{sep2}} \tag{24}$$

Once λ'^*_{sep} is found, it is numerically shown that $\Delta\tilde{V}^*$ is minimum when

$$\eta^* \approx 0.39$$

by simply scanning η.

Hence, the optimal separation impulse has been found almost completely analytically.

Geometrical Approach

The optimal consumption is known. However, we are also interested in the maneuvers' characteristics to assess the collision risk. For this problem, no straightforward solution using the primer vector alone has been found in the literature. The solution we propose is based on the method introduced by Baranov in Ref. 21: It consists of finding a geometrical solution compliant with the necessary conditions of optimality given by the primer vector. For the nondegenerate case, the first condition is that the solution be two impulsive. The second condition is that the direct cosines must be opposite, except for the transversal components, which must be equal.

For the first interval, that is, when $\lambda'^*_{\text{sep}}=\pi/2+\theta$, the separation impulse is applied along $\boldsymbol{\delta e}$. The corresponding geometrical solution compliant with the conditions of optimality is represented in Fig. 6. From Fig. 6, it follows that

$$\|\boldsymbol{\xi}_{rj}\| = \{-\|\boldsymbol{\delta e}\|/2 + \|\boldsymbol{\Delta}\tilde{\boldsymbol{V}}_{\text{sep}}\|[1-\sin(\lambda'_1-\theta)]\}/[\cos(\lambda'_1-\theta)]$$

$$\|\boldsymbol{\xi}_{tj}\| = \|\boldsymbol{\Delta}\tilde{\boldsymbol{V}}_{\text{sep}}\|, \qquad \|\boldsymbol{\xi}_{nj}\| = \|\boldsymbol{\delta i}'\| \,/\, 2\cos(\lambda'_1-\theta) \tag{25}$$

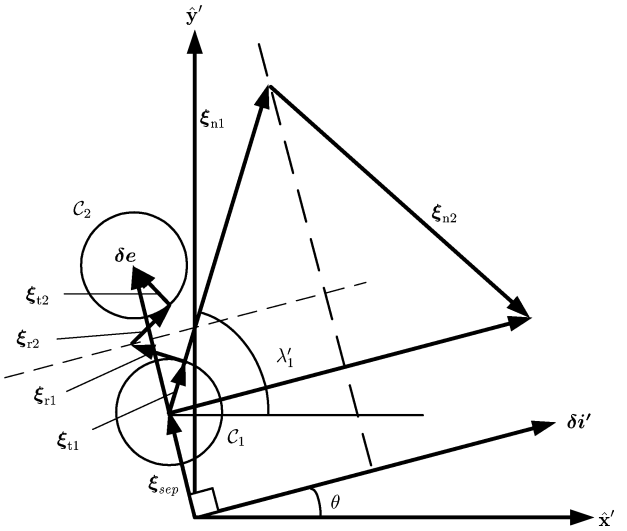

Fig. 6 Geometrical solution compliant with primer vector necessary conditions of optimality for first interval.

Given the fuel consumption

$$\Delta\tilde{V} = \sum_{j=1}^{2}\sqrt{\Delta\tilde{V}_{rj}^2 + \Delta\tilde{V}_{tj}^2 + \Delta\tilde{V}_{nj}^2} \tag{26}$$

the root of $\partial_{\lambda'_1}(\Delta\tilde{V})=0$ is found to be

$$\lambda'^*_1 = \arcsin\left[\frac{1-\eta+2\eta^2+\sqrt{1-2\eta+4\eta^2}}{\eta(2\eta-1)}\right]+\theta \tag{27}$$

for the circular formation, that is, $k_1=1$, and

$$\lambda'^*_1 = \arcsin\left[\frac{1}{4}\frac{5-4\eta+8\eta^2+\sqrt{5}\sqrt{5-8\eta+16\eta^2}}{\eta(2\eta-1)}\right]+\theta \tag{28}$$

for the projected circular formation, that is, $k_1=\sqrt{3}/2$.

This leads to the optimal solution,

$$\lambda'_1 = 2n_1\pi + \lambda'^*_1 + \pi, \qquad \lambda'_2 = 2n_2\pi + \pi - \lambda'^*_1 + 2\theta$$

$$\Delta\tilde{V}^*_{r1} = \{-\tilde{\rho}/4 + \|\boldsymbol{\Delta}\tilde{\boldsymbol{V}}_{\text{sep}}\|[1-\sin(\lambda'_1-\theta)]\}/[\cos(\lambda'_1-\theta)]$$

$$\Delta\tilde{V}^*_{r2} = -\Delta\tilde{V}^*_{r1}, \qquad \Delta\tilde{V}^*_{t1} = -\|\boldsymbol{\Delta}\tilde{\boldsymbol{V}}_{\text{sep}}\|/2$$

$$\Delta\tilde{V}^*_{t2} = \Delta\tilde{V}^*_{t1}, \qquad \Delta\tilde{V}^*_{n1} = -k_1\tilde{\rho}/2\cos(\lambda'_1-\theta)$$

$$\Delta\tilde{V}^*_{n2} = -\Delta\tilde{V}^*_{n1} \tag{29}$$

where n_1 and n_2 are integers.

In the same manner, the geometrical solution compliant with the conditions of optimality is represented in Fig. 7 for the second interval, that is, for which $\lambda'^*_{\text{sep}} = \arctan 1/\sqrt{(4\eta^2-1)}+\theta$. From Fig. 7, it follows that

$$\lambda'_1 = 2n_1\pi + \theta, \qquad \lambda'_2 = 2n_2\pi + \lambda'_1 + \pi$$

$$\Delta\tilde{V}^*_{r1} = 0, \qquad \Delta\tilde{V}^*_{r2} = 0$$

$$\Delta\tilde{V}^*_{t1} = -\sqrt{4\|\boldsymbol{\Delta}\tilde{\boldsymbol{V}}_{\text{sep}}\|^2 - \tilde{\rho}^2/4}\,\Big/\,4 - \|\boldsymbol{\Delta}\tilde{\boldsymbol{V}}_{\text{sep}}\|/2$$

$$\Delta\tilde{V}^*_{t2} = -\Delta\tilde{V}^*_{t1} - \|\boldsymbol{\Delta}\tilde{\boldsymbol{V}}_{\text{sep}}\|, \qquad \Delta\tilde{V}^*_{n1} = -k_1\tilde{\rho}\,/\,\|\boldsymbol{\Delta}\tilde{\boldsymbol{V}}_{\text{sep}}\|\Delta\tilde{V}^*_{t1}$$

$$\Delta\tilde{V}^*_{n2} = k_1\tilde{\rho}\,/\,\|\boldsymbol{\Delta}\tilde{\boldsymbol{V}}_{\text{sep}}\|\Delta\tilde{V}^*_{t2} \tag{30}$$

These solutions now permit assessment of the collision risk.

Collision Risk Assesment

Now a distance constraint between vehicles is needed:

1) Between a spacecraft and the rocket upper stage, once a spacecraft is separated, the distance to the rocket upper stage will initially increase due to the semimajor axis change. (The separation impulse is transversal.) One revolution after the separation, the distance will then reach a minimum. (See the example in Fig. 8.) This minimum must be greater than the constraint.

2) Between individual spacecraft, when the first spacecraft is separated, the distance to the next, which is not yet released, begins to increase. Then the distance will decrease because the next spacecraft is separated. The minimum distance is computed only once the first maximum is reached.

It can be demonstrated numerically that the minimum distances increase with η, that is, with the separation impulse amplitude. Furthermore, at the end of the optimization section, the optimal value of η is obtained for minimizing the fuel consumption.

Hence, the strategy is simple: A first run is made with the optimal value for η. The minimum distances are then computed. If they are greater than the constraint, then this solution is retained. If not, the separation impulse amplitude is increased starting from the optimal

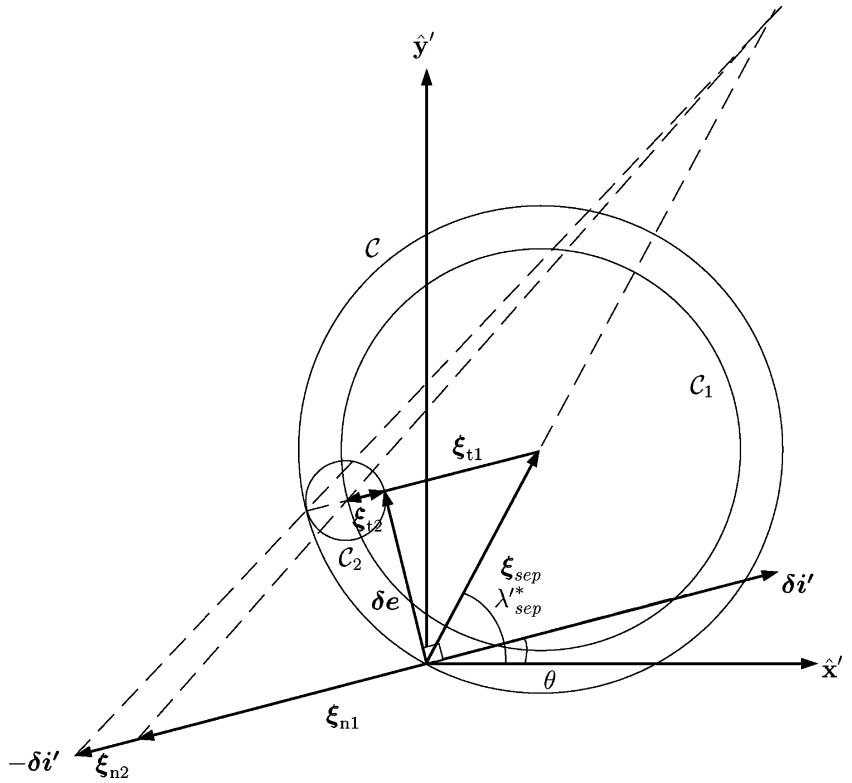

Fig. 7 Geometrical solution compliant with primer vector necessary conditions of optimality for the second interval.

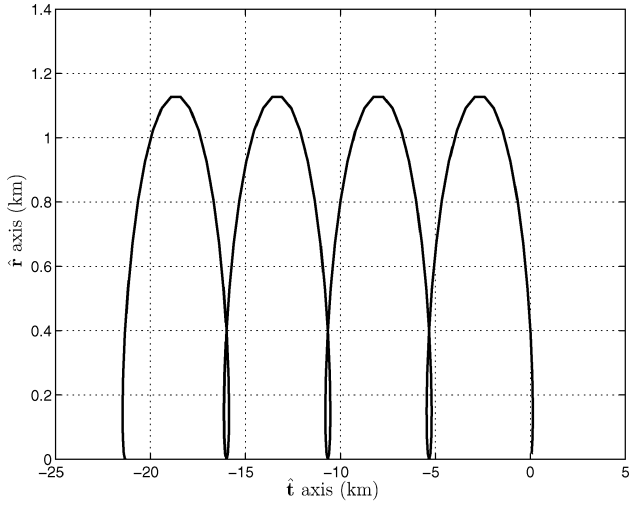

Fig. 8 Minimum distance between spacecraft and rocket upper stage; rocket upper stage altitude 700 km along circular orbit, transversal separation impulse amplitude 30 cm/s, relative trajectory represented in radial/transversal local orbital frame of the rocket upper stage during four revolutions, and minimum distance 5.330 km.

value until the constraint is met. The additional fuel consumption represents the constraint cost.

Numerical Example

Missions such as georeferencing or moving target identification can be regarded as pertinent study cases.[1] For such applications, spacecraft can fly in circular formations.

We consider a formation of five spacecraft initially stacked on the rocket upper stage. The target circular formation size parameter is $\rho = 2$ km. Without loss of generality, our study will focus on the first two spacecraft: Their phase angles are chosen to be $\theta_1 = 0$ deg and $\theta_2 = 72$ deg, which corresponds to a five spacecraft regular formation. The rocket upper stage orbital parameters are summarized in Table 1. The results of the formation design section allow the targeted changes in the spacecraft orbital elements to be derived, which are also given in Table 1.

Table 1 Formation design: rocket upper stage and spacecraft orbital parameters

Upper stage	Spacecraft 1	Spacecraft 2
$\bar{a} = 7200, 55$ km	$\delta a_1 = 0$ km	$\delta a_2 = 0$ km
$\bar{e} = 1.10^{-3}$	$\delta e_1 = 1.39^{-4}$	$\delta e_2 = 5.13^{-5}$
$\bar{i} = 55$ deg	$\delta i_1 = 1.38^{-2}$ deg	$\delta i_2 = 4.26^{-3}$ deg
$\bar{\Omega} = 0$ deg	$\delta\Omega_1 = 0$ deg	$\delta\Omega_2 = 1.60^{-2}$ deg
$\bar{\omega} = 90$ deg	$\delta\omega_1 = 0$ deg	$\delta\omega_2 = 7.218$ deg
$\bar{M} = 0$ deg	$\delta M_1 = 0$ deg	$\delta M_2 = -7.227$ deg

The deployment is supposed to be constrained by the minimum distance $d_{\min}$. The task is solved for two values: $d_{\min} = 1$ and 1.5 km.

It has been found in Ref. 12 that n_{sep} and n_1 [definitions in Eqs. (22) and (29)] can be properly chosen. Given n_{sep1} for the first spacecraft, the minimum distance with the other spacecraft is increased[12] if

$$n_{\text{sep2}} - n_{\text{sep1}} = 1 \tag{31}$$

Furthermore, the minimum distance with the rocket upper stage is increased if

$$n_1 - n_{\text{sep}} = 1 \tag{32}$$

The main results of the optimization process are given in Table 2. Two variables are introduced for comprehension purposes: η_r and η_{sc}. They correspond to the minimum value for η to be compliant with the constraint: If $\eta > \eta_r$ (respectively, η_{sc}) then the minimum distance between one spacecraft and the rocket upper stage (respectively, the other spacecraft) will be greater than $d_{\min}$.

Note that all numerical simulations show that $\eta_{\text{sc}} > \eta_r$. This means that it is sufficient to focus on the distance between spacecraft: The other distance constraint will be always satisfied. Furthermore, for

Table 2 Optimal deployment results for two minimum-distance constraints

Parameter	$d_{\min} = 1$ km	$d_{\min} = 1.5$ km
η_r	0.06	0.1
η_{sc}	0.18	0.71
$\eta_{\min}$	0.18	0.71
η^*	0.39	0.71
$\|\Delta V_{sep}\|$, cm/s	40.30	73.65
$\|\Delta V\|$, m/s	1.85	1.93
Cost, %	0	4.32

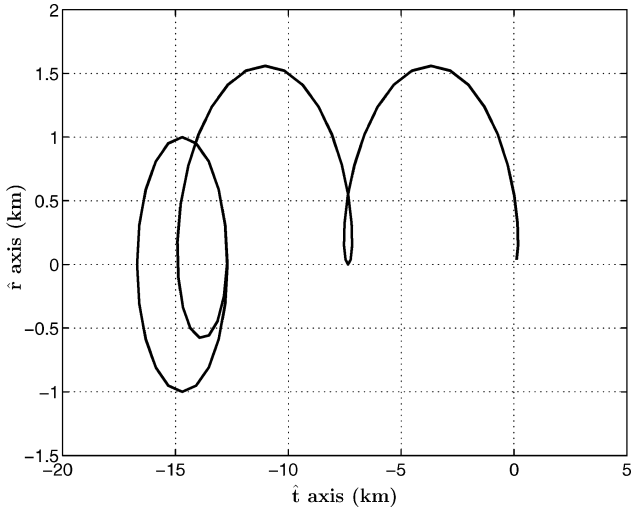

a) Projection onto transversal–radial plane

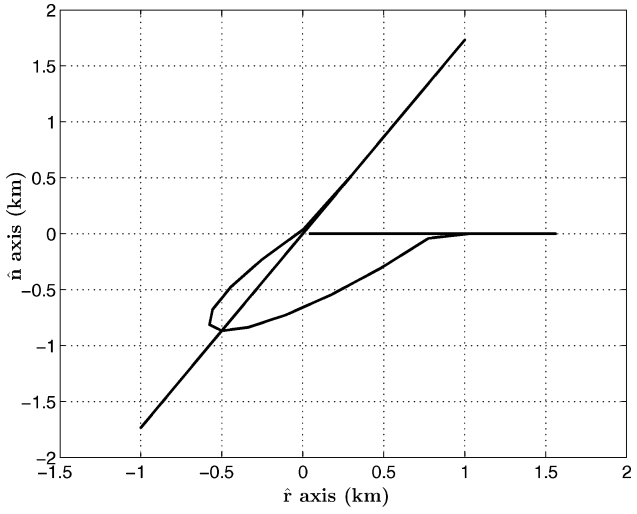

b) Projection onto transversal–normal plane

Fig. 9 Motion of a spacecraft with respect to rocket upper stage.

$d_{\min} = 1$ km, $\eta_{sc} < \eta^*$. Hence, if η^* is taken to calculate the separation impulse, the fuel consumption is reduced while still satisfying the distance constraint. However, for $d_{\min} = 1.5$ km, $\eta_{sc} > \eta^*$. The optimal value η^* cannot be used because the constraint would be violated. In this case, η_{sc} must be used to compute the separation impulse. The fuel consumption will not be optimal. Then the cost with respect to the optimal case can be derived. As a consequence, these results show that the optimal value η^* corresponds to a minimum distance $d^*_{\min}$ that lies between 1 and 1.5 km.

Suppose now that η_{sc} and η_r are unknown. (This is actually the case.) A first run is made with η^*. The optimal minimum distance $d^*_{\min}$ is derived. Because $d^*_{\min} > d_{\min}$ for the first case, the optimal solution is kept. However, for the second case, we have $d^*_{\min} < d_{\min}$. Hence, η is increased until the constraint is met and so η_{sc} is found.

From Table 2, the optimal separation impulse amplitude is roughly 40 cm/s for the first case. When compared with the Gravity Recovery and Climate Experiment mission deployment,[16] for which the separation impulse is 28 cm/s, this result seems to be realistic. The optimal deployment fuel consumption is 1.85 m/s, which is reasonable for a microsatellite platform. For the second case, the separation amplitude doubles, and the fuel consumption increases by 8 cm/s. This extra fuel consumption corresponds to the constraint cost and amounts to 4% of the optimal consumption.

Figure 9 illustrates the trajectory of the two spacecraft during the deployment in the LOF of the rocket upper stage for the case $d_{\min} = 1$ km. Figure 9a is the projection onto the transversal–radial plane, whereas Fig. 9b is the projection onto the transversal–normal plane. As stated earlier, the optimal solution is the same for all spacecraft; the only difference is the different separation time. Then the two trajectories are the same in the LOF of the rocket upper stage. The minimum distance between each spacecraft and the rocket upper stage can be derived from Fig. 9, as shown in Fig. 8.

Figure 10 relates to the evolution of the distance between the two spacecraft. Figure 10a represents the evolution of the distance between them as a function of time. First, because the formation is circular, the final distance is constant. Furthermore, the minimum distance is reached just before the end of the deployment. To illustrate this feature, Fig. 10b shows the trajectory of the two spacecraft in the transversal–radial plane as a function of time. Note that the minimum distance is reached when the second spacecraft is inserted into the formation.

Finally, Fig. 11 illustrates the solution proposed in this paper. It is a snapshot during the deployment of three spacecraft.

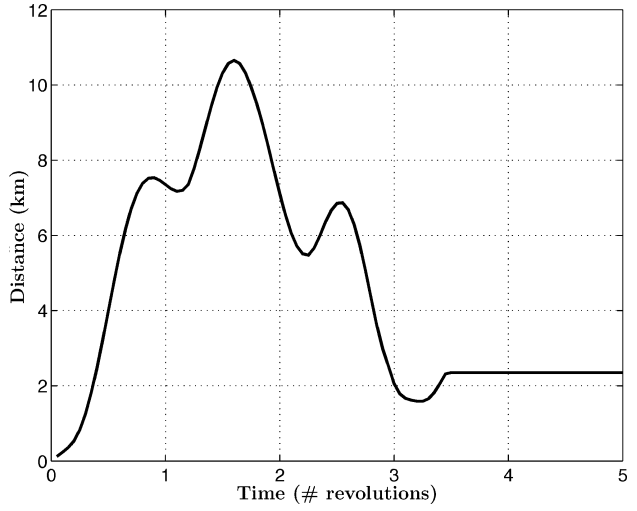

a) Distance between two spacecraft

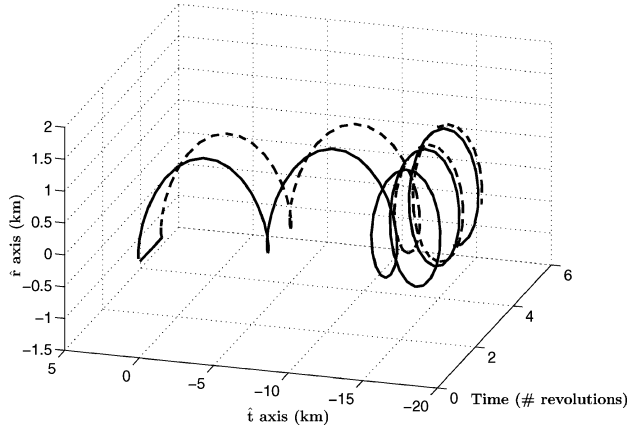

b) Spacecraft trajectories in transversal–radial plane as function of time

Fig. 10 Relative motion between two spacecraft.

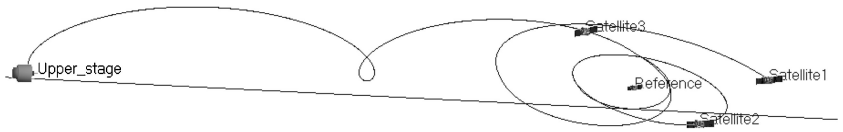

Fig. 11 Deployment solution for four-spacecraft formation, one already flying around a reference spacecraft; two others are about to begin their relative circular motion.

Conclusions

This paper presents new results related to the deployment of invariant formations. Before solving the optimization problem, an innovative model for the formation design is introduced. This model allows management of near-circular and near-equatorial reference orbits. It also complies with the inputs required by the employed optimization method.

Then the minimum fuel consumption for the formation deployment is obtained via the primer vector optimal control theory. The deployment strategy includes a separation impulse by the rocket upper stage. The optimal time application and magnitude of the impulse are obtained analytically. Then the two-impulse optimal solution is analytically derived by combining the primer vector results with a geometrical approach. This permits assessment of the collision risk by observing the evolution of the distance between spacecraft.

It is shown that introducing a minimum-distance contraint can incur a fuel penalty when it exceeds a limit value.

Finally, we arrive at an almost fully analytical solution to the problem of invariant formation deployment.

Acknowledgments

We are grateful to P. Brousse, E. Lansard, and T. Dargent for their technical support. We also acknowledge M. Bousquet for his precious help. Many thanks to M. Khan for the improvement of the revised version.

References

[1]Kong, E., Miller, D., and Sedwick, R., "Exploiting Orbital Dynamics for Aperture Synthesis Using Distributed Satellite Systems: Application to a Visible Earth Imager System," *Journal of Astronautical Sciences*, Vol. 47, No. 1–2, 1999, pp. 53–75.

[2]Boutonnet, A., Escudier, B., and Martinot, V., "Direct Approach for Spacecraft Formation-Flying Positioning in Quasicircular Low Earth Orbit," AIAA Paper 2002-4638, Aug. 2002.

[3]Scharf, P., Hadaegh, F. Y., and Kang, B. H., "A Survey of Spacecraft Formation Flying Guidance," *Proceedings of the International Symposium on Formation Flying Missions and Technologies*, Paper 4.1, Centre National d'Etudes Spatiales, Toulouse, France, Oct. 2002.

[4]Schaub, H., and Alfriend, K. T., "Impulsive Feedback Control to Establish Specific Mean Orbit Elements of Spacecraft Formations," *Journal of Guidance, Navigation, and Control*, Vol. 24, No. 4, 2001, pp. 739–745.

[5]MacLaughlin, C. A., Alfriend, K. T., and Lovell, T. A., "Analysis of Reconfiguration Algorithm for Formation Flying Experiments," *Proceedings of the International Workshop on Formation Flying Missions and Technologies*, Paper 1.2, Centre National d'Etudes Spatiales, Toulouse, France, Oct. 2002.

[6]Vaddi, S. S., Alfriend, K. T., and Vadali, S. R., "Sub-Optimal Formation Establishment and Reconfiguration Using Impulsive Thrust," *Advances in Astronautical Sciences*, Vol. 116, 2003, pp. 1419–1436.

[7]Sabol, C., Burns, R., and McLaughlin, C. A., "Satellite Formation Flying Design and Evolution," *Journal of Spacecraft and Rockets*, Vol. 38, No. 2, 2001, pp. 270–278.

[8]Vadali, S. R., Vaddi, S. S., and Alfriend, K. T., "A New Concept for Controlling Formation Flying Satellite Constellations," *Advances in Astronautical Sciences*, Vol. 108, 2001, pp. 1631–1648.

[9]Mishne, D., "Formation Control of LEO Satellites Subject to Drag Variations and J2 Perturbations," *Journal of Guidance, Control, and Dynamics*, Vol. 27, No. 4, 2004, pp. 685–692.

[10]Kemble, S., and Swinburne, B., "Design of Satellite Formations in Low Earth Orbit and Deep Space," International Aeronautical Federation, World Congress, Paper IAC-02-A.2.03, Oct. 2002.

[11]Battin, R. H., *An Introduction to the Mathematics and Methods of Astrodynamics*, AIAA Education Series, AIAA, New York, 1987, pp. 203–212.

[12]Boutonnet, A., Baranov, A., Martinot, V., Escudier, B., and Noailles, J., "Optimal Circular Formation Initialization with Collision Risk Management," *Advances in Astronautical Sciences*, Vol. 116, 2003, pp. 2385–2402.

[13]Boutonnet, A., Martinot, V., Brousse, P., and Escudier, B., "Efficient and Accurate Satellite Formation Flying Positioning in Low Earth Orbit," *Proceedings of the International Symposium on Formation Flying Missions and Technologies*, Paper 4.5, Centre National d'Etudes Spatiales, Toulouse, France, Oct. 2002.

[14]Boutonnet, A., Martinot, V., Baranov, A., Escudier, B., and Noailles, J., "Optimal Analytical Solution for Invariant Spacecraft Formation Initialization," *Proceedings of the Third International Workshop on Satellite Constellations and Formation Flying*, CNR, Pisa, Italy, 2003, pp. 197–206.

[15]Carrou, J. P., *Space Mechanics*, Cepadues-Editions, Toulouse, France, 1995, Chap. 6.

[16]Kirschner, M., "First Results on the Implementation of the GRACE Formation," *Proceedings of the Third International Workshop on Satellite Constellations and Formation Flying*, CNR, Pisa, Italy, 2003, pp. 263–269.

[17]Vincent, M., and Salcedo, C., "The Insertion of Cloudsat into the A-Train Constellation," *Advances in Astronautical Sciences*, Vol. 116, 2003, pp. 1401–1418.

[18]Lawden, D. F., *Optimal Trajectories for Space Navigation*, Butterworths, London, 1963.

[19]Edelbaum, T. N., "Minimum Impulse Transfers in the Near Vicinity of a Circular Orbit," *Journal of Astronautical Sciences*, Vol. 14, No. 2, 1967, pp. 66–73.

[20]Marec, J. P., *Optimal Space Trajectories*, Elsevier, Amsterdam, 1979, Chap. 7.

[21]Baranov, A. A., "Geometric Solution of the Problem of a Rendezvous on Close Nearly Circular Coplanar Orbits," *Cosmic Research*, Vol. 27, No. 6, 1989, pp. 682–696.

J. Korte
Associate Editor